ACS APPLIED MATERIALS & INTERFACES

Research Article

www.acsami.org

Simple, Large-Scale Patterning of Hydrophobic ZnO Nanorod Arrays

Seong Been Kim,[†] Won Woo Lee,[†] Jaeseok Yi,[†] Won Il Park,[†] Jin-Sang Kim,[‡] and William T. Nichols*[,†]

[†]Division of Materials Science and Engineering, Hanyang University, Seoul 133-791, Korea

[‡]Electronic Materials Research Center, Korea Institute of Science and Technology, Seoul 136-791, Republic of Korea

ABSTRACT: Here we describe a simple, versatile technique to produce large-scale arrays of highly ordered ZnO nanorods. Patterning of three distinct ZnO crystal morphologies is demonstrated through use of different ZnO seed layers. Array formation is accomplished through a simple variation on nanosphere lithography that imprints a thickness variation across a PMMA mask layer. The area of exposed seed layer is controlled through etching time in an oxygen plasma. Subsequent hydrothermal growth from the patterned seed layer produces high-quality ZnO crystals in uniform arrays. The high uniformity of the patterned array is shown to induce a high contact angle hydrophobic state even without the need for chemical modification of the ZnO surface. This technique provides a straightforward way to integrate the optical and electrical properties of high-quality ZnO nanorods with the tunable fluidic properties at the surface of well-ordered arrays.

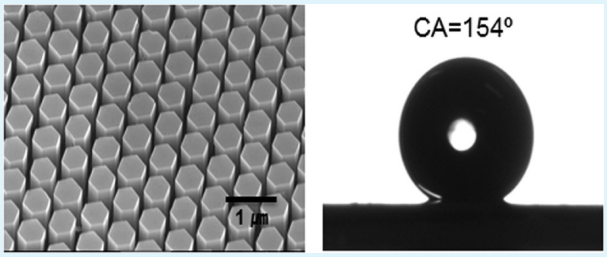

KEYWORDS: *ZnO nanorods, hydrothermal, nanosphere lithography, hydrophobic*

1. INTRODUCTION

One-dimensional nanostructured ZnO materials display enhanced light absorption and extraction; improved charge transport and large surface to volume ratio making them excellent candidates for electronic, optoelectronic, electrochemical, and electromechanical devices.[1−3] Vertical alignment of the ZnO nanorods further expands potential applications due to the higher element density. This has enabled the development of quasi-3D structured devices such as LEDs, laser diodes, vertical FETs, biochemical sensors and photovoltaic cells.[4−8] More recently, the challenge has become to synthesize well-ordered vertically aligned nanorod arrays because the uniform separation and high symmetry can induce collective behavior among the nanorods in the array. Potential applications of this emergent behavior include photonic crystals for light transport[9−11] and designed surfaces for micro-control of liquid at interfaces.[12,13]

A variety of patterning approaches have been introduced to achieve vertically aligned ZnO nanorod arrays such as electron-beam lithography and laser-interference lithography.[9,10,14] These nanoscale lithographic techniques produce arrays of excellent uniformity, however, they require expensive facilities and complex processing. In recent years nanosphere lithography (NSL) has emerged as a promising alternative capable of high-precision wafer-scale hexagonal-patterned arrays from which ZnO nanostructures can be grown. Typically, NSL patterning has been used in conjunction with vapor phase synthesis of ZnO nanostructures.[15−18] The need for vacuum processing and ZnO crystal contamination by the metal catalyst has encouraged the search for an improved synthesis technique. Recently, hydrothermal synthesis has shown promise as a simpler, more controllable technique.[19,20] Preliminary work has produced good results, however, there are still two primary drawbacks. First, ZnO crystal growth is generally initiated from a heterogeneous single crystal substrate. This limits the achievable crystal morphologies and orientations. Second, inorganic sols are frequently used to transfer the nanosphere pattern to the substrate. The inorganic sol is difficult to remove and may interfere with some potential applications.

Here we demonstrate a simple technique that simultaneously satisfies three critical design principles: (i) growth of high-quality ZnO nanorods of controllable morphology; (ii) patterning into uniform, well-ordered arrays; (iii) use of a simple, low-cost process. The crystal morphology is controlled through selection of an appropriate ZnO seed layer. Patterning is accomplished through a simple variation on nanosphere lithography that creates a topographical thickness variation across a PMMA mask layer. The area of exposed seed layer is controlled through etching time in an oxygen plasma. Subsequent hydrothermal growth produces high quality nanorods patterned into uniform arrays. The high uniformity of the array is indicated by the transition to a high contact angle hydrophobic surface state even without chemical modification. This work expands the possibilities for the integration of the excellent optical and electrical properties of high-quality ZnO nanorods with fluidic technologies for applications such as waterproof optoelectronics and opto-fluidics.

2. EXPERIMENTAL SECTION

The process flow for fabrication of patterned ZnO nanorod arrays is shown in Figure 1. Three different types of ZnO seed

Received: April 23, 2012
Accepted: June 26, 2012
Published: June 26, 2012

   dx.doi.org/10.1021/am3007142 | ACS Appl. Mater. Interfaces 2012, 4, 3910−3915

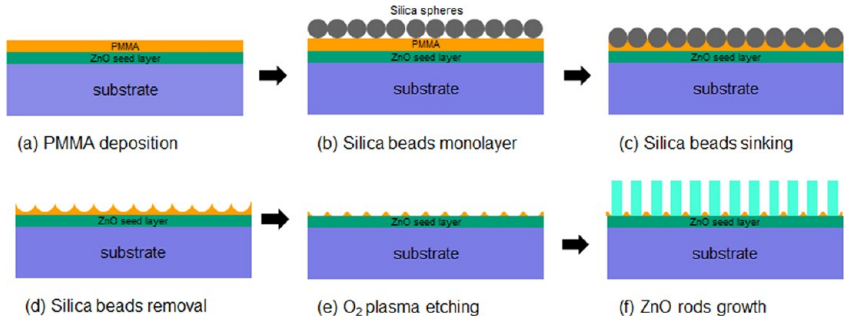

Figure 1. Schematic illustrating the patterning process to produce well-ordered, vertically aligned ZnO nanorods.

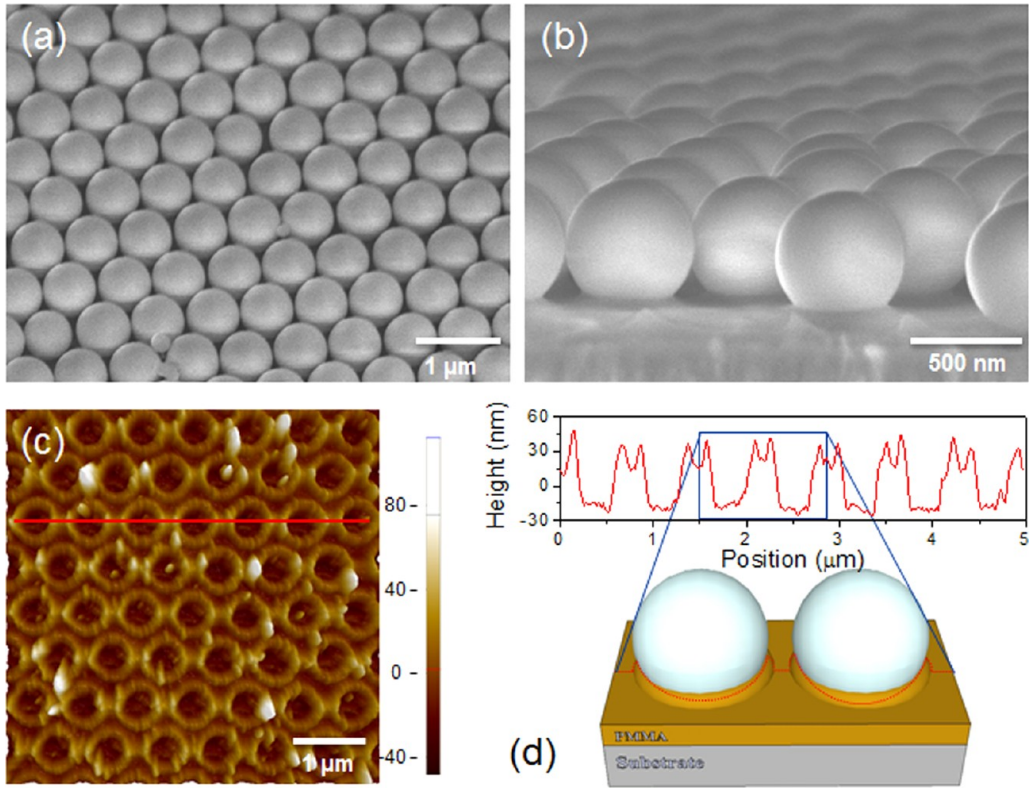

Figure 2. Topographical patterning of the PMMA etch mask: (a) top-view SEM of self-assembled silica spheres; (b) cross-sectional view showing an silica sphere sunk into the PMMA layer; (c) AFM topography of the PMMA layer after removal of the silica spheres; (d) AFM surface profile and schematic showing the sunken central depressions and the raised meniscus outer rings.

layers were studied and will be referred to by the type number in the text. Type I seed layers were prepared by RF magnetron sputtering of a stoicheometric ZnO target onto the native oxide of a silicon wafer. Type II seeds were prepared on a clean Si(100) wafer by pulsed laser deposition. Type III seeds were grown epitaxially by pulsed laser deposition on Al_2O_3 (0001) substrates. Detailed crystallographic analysis of the ZnO seed layers and resulting ZnO nanorod structures were reported previously.[14]

Patterning is accomplished by first spin coating a 200 nm layer of poly(methyl methacrylate) (PMMA) over the ZnO seed film. The PMMA is briefly exposed to an oxygen plasma (30 W, 3 sec) to transform the initial hydrophobic surface into a hydrophilic surface. On the PMMA-coated substrates, a hexagonally close-packed monolayer of silica spheres is deposited by Langmuir-Blodgett assembly (Figure 1b). Next, the samples are heated to 180°C for 4 min to soften the PMMA and allow the silica spheres to sink down into the polymer layer. The embedded silica spheres are removed via chemical etching with a diluted hydrofluoric acid solution (H_2O:HF = 50:1). The resulting topographical pattern in the PMMA layer consists of a hexagonal-array of circular depressions surrounded by raised meniscus rings caused by capillary wetting around the spheres (Figure 1d). A mild etch of the PMMA layer with an oxygen plasma (30 W, 5−20 s) erodes the PMMA layer exposing the underlying ZnO seeds to an extent that is controlled by the etching time (Figure 1e).

Following patterning, ZnO nanostructures are grown from the exposed seed areas by hydrothermal synthesis using a standard recipe.[21] Briefly, the patterned substrates are placed in an aqueous solution containing (0.025 M) zinc nitrate hexahydrate ($Zn(NO_3)_2$ $6H_2O$, Sigma-Aldrich) and (0.025 M) hexamethylenetetramine ($C_6H_{12}N_4$, Sigma-Aldrich). The equimolar solution is placed in an oven at 90 °C for 12 h creating well- ordered, vertically aligned ZnO nanostructures (Figure 1f). The PMMA mask remains after the hydrothermal

dx.doi.org/10.1021/am3007142 | ACS Appl. Mater. Interfaces 2012, 4, 3910−3915

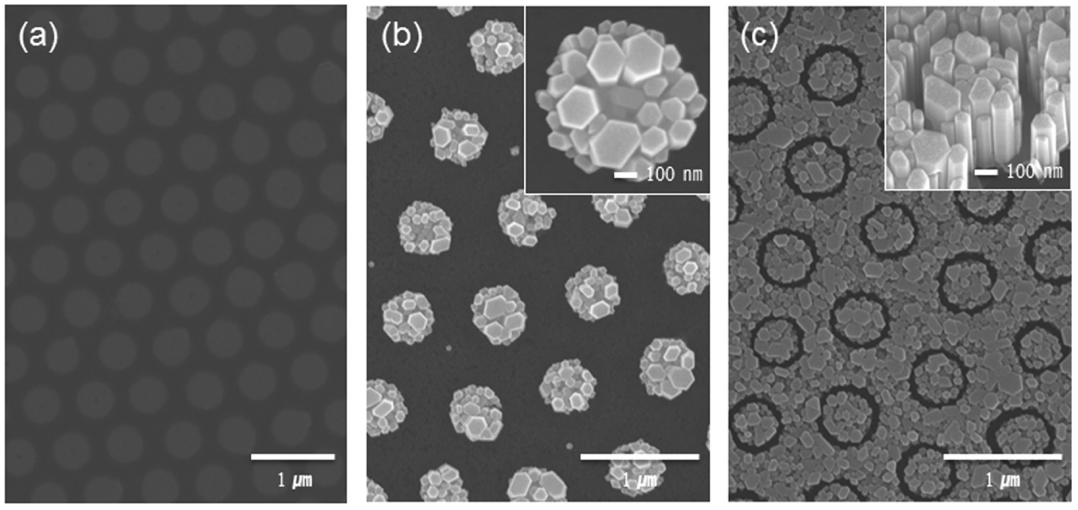

Figure 3. Etching control of the PMMA mask: (a) under etching with no exposure of the underlying ZnO seed layer and no subsequent growth of ZnO nanorods; (b) appropriate etching to expose central regions of the pattern and growth of circular ZnO nanorods; (c) excessive etching leaving only PMMA in the outer meniscus rings.

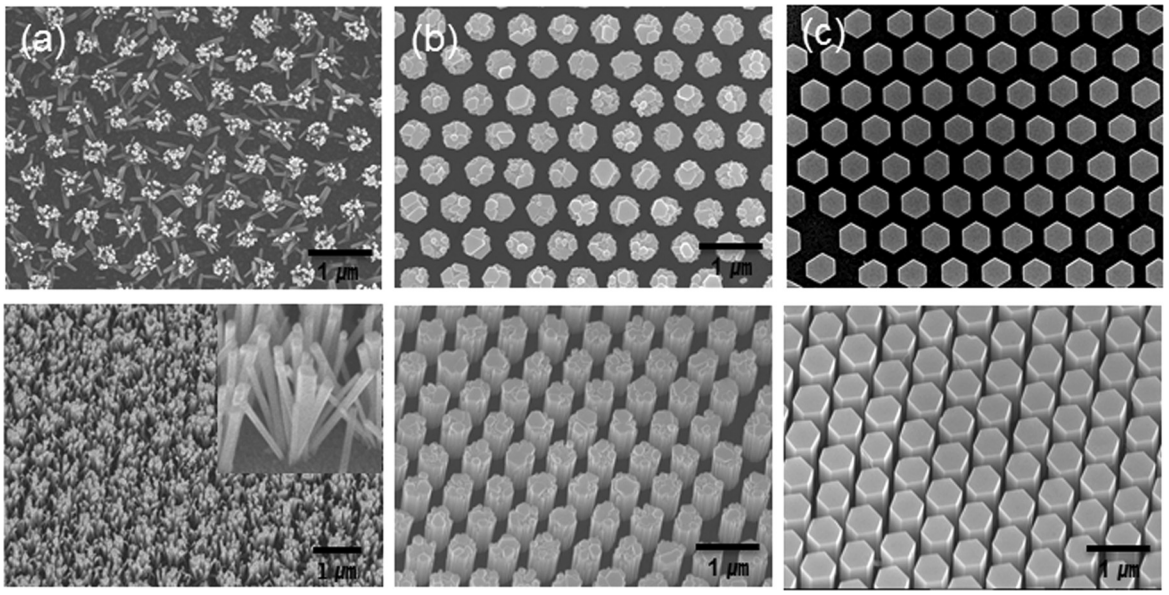

Figure 4. Growth of three types of ZnO nanorod patterns: (a) type I nanoflowers lacking both in-plane and *c*-axis orientation; (b) type II multidomain columns with good c-axis orientation, but lacking in-plane orientation; (c) type III single crystal columns with both excellent in-plane and *c*-axis orientation.

growth and can be removed by a short O_2 plasma etch, though this step was not carried out on the samples reported here. The resulting samples were washed in deionized water and analyzed microscopically via field-emission scanning electron microscopy (FE-SEM, JEOL JSM-7600F) and atomic force microscopy (AFM, Park Systems, XE-100). The surface wetting properties were measured by a water contact angle system (Contact Angle Meter, GBX-DigiDrop).

3. RESULTS AND DISCUSSION

Figure 2 shows the hexagonally close-packed monolayer of silica spheres and the subsequent PMMA topographical patterns. When heated to 180 °C the PMMA softens and the silica spheres sink down into the polymer layer as shown in Figure 2b. After removal of the silica spheres, the resulting surface topography exhibits a uniform pattern of circular depressions surrounded by raised meniscus rings. The depth of the depressions are ~40 nm below and the meniscus rings peak up ~20 nm above the original surface level (Figure 2d).

An oxygen plasma is used to etch the PMMA layer. Because of the patterned thickness variations, etching time sensitively tunes the area of the underlying seed layer that is exposed (Figure 3). If the etching time is insufficient (time <8 s), a continuous layer of PMMA remains across the surface fully masking the seeds and preventing ZnO nanorod growth (Figure 3a). With an appropriate etching time (8−13 s), circular regions of the seed layer are exposed from which ZnO nanostructures are grown (Figure 3b). Control of the ZnO nanostructure size therefore, can be accomplished by a combination of two factors. First, the size of the original silica spheres sets the overall lattice spacing of the array. Second, the degree of etching sets the size of the individual nanostructures within the pattern. Finally, in the case of over-etching ($t \approx 13$

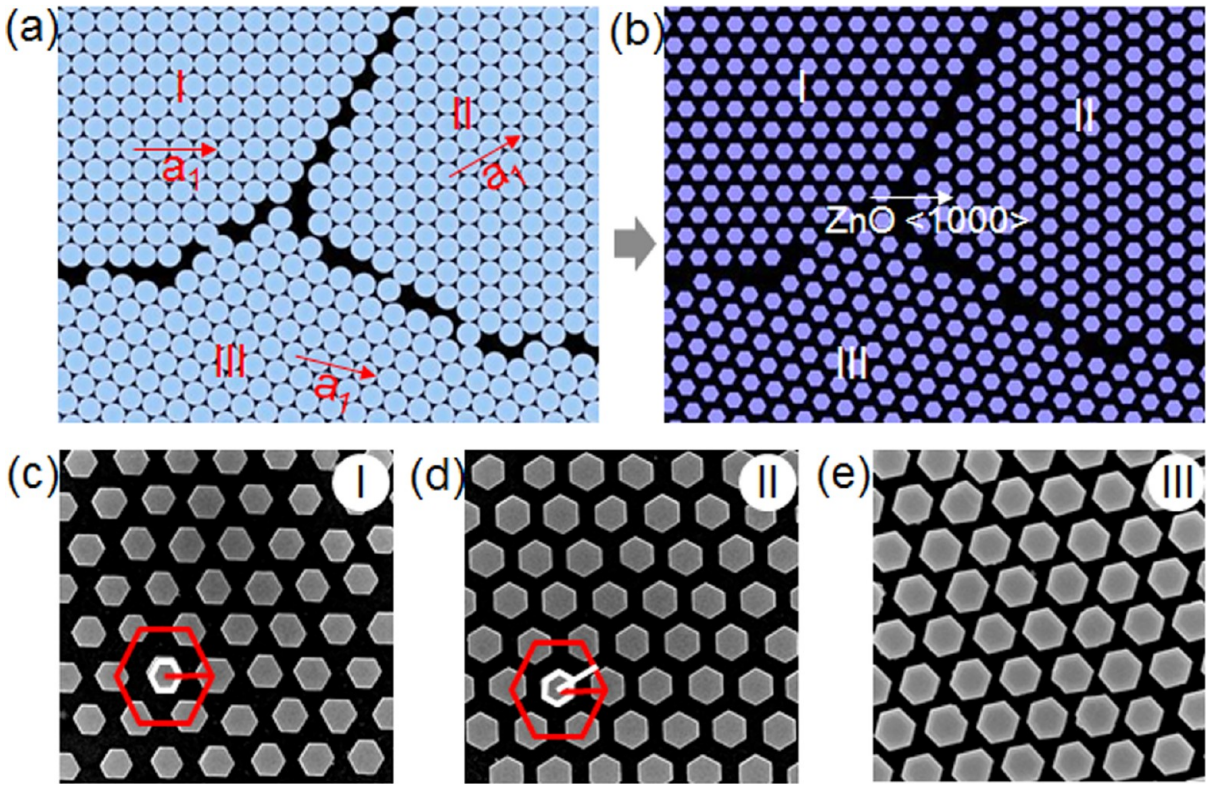

Figure 5. Orientational control of the ZnO patterns: (a) SEM of self-assembled silica spheres showing three regions with different relative orientation between the hexagonal sphere pattern and the underlying ZnO seed in-plane orientation, (b) ZnO nanorods grown from the pattern shown in a; (c–e) magnified SEM images of ZnO nanorods with different orientations within the array: (c) the ZnO ⟨1000⟩ crystal vector is parallel with the ⟨1000⟩ direction of the overall hexagonal array; (d) ZnO ⟨1000⟩ crystal is rotated by 30° compared to the array's hexagonal lattice; (e) an intermediate angle between 0 and 30°.

s), most of the PMMA can be removed except the raised meniscus rings. Growth from this mask produces well-ordered, circular wells surrounded by a continuous ZnO nanorod layer (Figure 3c). This form holds the liquid in nano-scale contact with the ZnO and might find applications in nanowell analytical sensors or catalytic nanoreactors for fine chemical synthesis.[22,23]

A key advantage of this technique is the utilization of a ZnO seed layer to initiate the nanorod growth. The seed layer both enables the selection of the desired crystal morphology within the pattern and promotes high-quality crystallization. To illustrate this point, we grew patterned arrays from three distinct seed layers with different *c*-axis and in-plane crystallographic orientations. Type I seeds lack both in-plane and *c*-axis orientation. The resulting bundles of radially protruding nanorods resemble nanoflowers as seen in Figure 4a. Type II seed films have good *c*-axis orientation, but lack in-plane orientation. Hydrothermal growth from this patterned seed layer produces arrays of multidomain columnar structures (Figure 4b). Type III epitaxial seed films display both *c*-axis and in-plane orientations. The resulting arrays are composed of single-crystal ZnO columns with well–defined hexagonal facets (Figure 4c). Taken together, Figures 3 and 4 show that this technique enables the independent optimization of both the individual ZnO nanorod units and the overall patterning of these units into arrays. Moreover, this technique has potential to be scaleable due to the ability to create large-scale nanosphere patterns with the Langmuir–Blodgett assembly technique coupled with the ability to grow the high-quality nanorod arrays hydrothermally at low temperature in ambient pressure ovens.

Collective properties will depend on the orientation of the individual hexagonal nanorods within the array. Figure 5 shows a fortuitous region illustrating the range of possible orientations of the individual ZnO nanorods with respect to the overall hexagonal symmetry of the array. When the in-plane crystal orientation of the seed coincides with the orientation of the silica sphere array, the resulting ZnO nanorods have the same orientation as the overall pattern as noted in region I (Figure 5c). When the in-plane crystal orientation of the seed is rotated by 30° with respect to the hexagonal arrangement of spheres as seen in region II, the result is an inverse honeycomb structure (Figure 5d). For the general case of angles between 0 and 30° (region III), intermediate orientations are observed (Figure 5e). Orientational control of the individual ZnO nanorod units relative to the overall symmetry may prove useful for defining the photonic or electrical coupling among the arrays. It may also be possible to use these patterns to control particle movement over the surface, e.g., in microfluidic particle or cell sorting.[24,25]

Zinc oxide nanorod arrays with excellent pattern uniformity enable the surface to display emergent properties. A prime example is the emergence of a hydrophobic wetting state from a hydrophilic material through surface texturing. This transition is demonstrated for the patterned ZnO nanorod arrays in Figure 6. Wettability of a surface depends on both the intrinsic surface affinity for the liquid and the surface texture. Zinc oxide is intrinsically hydrophilic and films of all three types of ZnO seed layers show similar values for the static water contact angle, CA

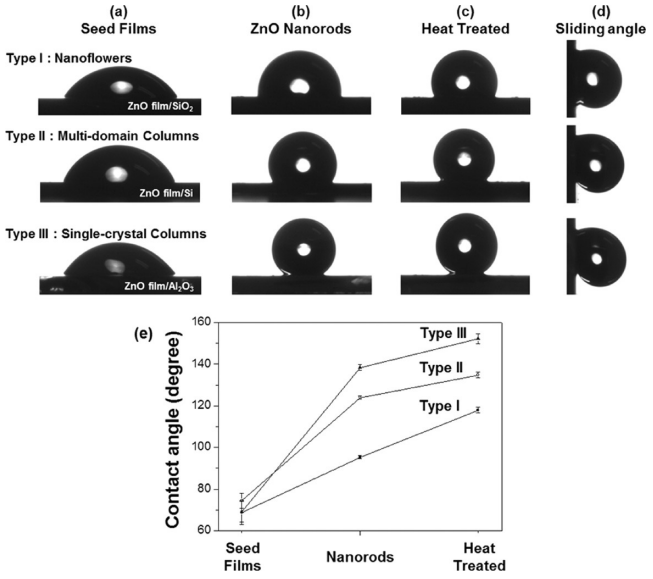

Figure 6. Water contact angle measurements for the three types of patterned ZnO nanostructures: (a) bare ZnO seed films; (b) as-grown ZnO nanostructures; (c) ZnO nanostructures after thermal treatment; (d) water adhesion on substrates inclined at a 90° angle. (e) Corresponding water contact angle graph.

≈ 68−75°. Growth of ZnO nanorod arrays introduce significant surface texturing that strongly increases the contact angle for all three ZnO nanostructure morphologies (Figure 6b). Heating the nanorod arrays at 150 °C was found to increase the contact angle in all three ZnO topographies (Figure 6c). When dynamic wetting tests were carried out, all samples showed a large CA hysteresis with significant water adhesion as demonstrated in Figure 6d for substrates tilted at a 90° angle. The quantitative trends in the contact angle of the surfaces are shown in Figure 6e.

Surface wetting properties are determined through a combination of the intrinsic surface energy of the ZnO facet in contact with the water and the surface texture.[26] The wurtzite structure of the ZnO nanorods consists of alternating zinc and oxygen atomic layers along the c-axis. The minimum energy is a top surface terminated by Zn+ ions, leaving a polar surface with large affinity for polar water molecules.[27] The non-polar side facets are generally terminated with hydroxyl groups providing a moderately hydrophilic surface in their initial state.[28] Additionally, the surface texture plays an important role in the surface wetting.[29−31] In the Wenzel state, water remains in full contact with the rough surface increasing the total surface area and amplifying the intrinsic surface properties. When air becomes trapped within the topographical features, however, the surface area decreases and is replaced with the perfectly hydrophobic air−water interface. In this Cassie state, the hydrophobicity of the surface increases to the extent that the effective surface area is reduced.

From this background, it is possible to interpret the wetting behavior and water adhesion of the three types of ZnO nanorod structures. Type I nanoflowers are composed of narrow rods with irregular spacing and poor vertical orientation resulting in little air trapping. Water penetrates into the spaces between rods and the surface exists in the Wenzel state. On the other hand, both type II multi-domain columns and Type III single-crystal columns are vertically oriented and able to trap air leading to a more pronounced hydrophobicity (CA of 122 and 137°, respectively). The ability to trap air suggests that the vertically aligned nanorod arrays are in the Cassie state. This is supported by the observation that when the water droplet is pushed into the surface the CA abruptly decreases because of air being forced out of the interconnected channels between the nanorods. Heating the ZnO nanorod arrays alters the surface energies by driving the terminal OH groups from the ZnO facets making them more hydrophobic. Type I nanoflowers show the largest improvement upon heating because in the Wenzel state the side facets are in contact with the water. Type II and Type III vertical nanorods show a more modest CA improvement because the top surface still has a strong affinity for the water, but air trapping is promoted by more hydrophobic side facets leading to less water penetration between the nanorods. The surface affinity also explains the large surface adhesion. In all three types of ZnO nanorod arrays, the top facet is terminated by Zn+ ions, which will electrostatically attract the water dipole, leading to strong adhesion despite the large contact angle as observed in Figure 6d.

The natural Lotus leaf uses two important design strategies: strongly hydrophobic surface coating and multi-scale structure to amplify the hydrophobic properties.[32] The static water contact angle of the Type III single crystal nanorod arrays (CA ≈ 154°) approach that of the Lotus leaf (CA ≈ 160°) despite having no hydrophobic surface modification. Previous work on ZnO surfaces designed using the Lotus principles has achieved contact angles up to 170°.[33−36] Because of the low surface energy of the hydrophobic coating, water droplets have a low adhesion leading to the self-cleaning properties of the Lotus effect. In contrast, our surfaces display both a large contact angle and high surface adhesion as have been observed for titania and zinc oxide designed surfaces.[37−39] In this work, the lack of a chemically modified surface allows the direct contact between the ZnO nanorods and liquid. This enables the electrical, optoelectronic and chemical functionality of the high quality nanorod arrays to interact directly with the liquid at the surface. The high CA and large adhesion enables the localization of liquid droplets on the surface even when tilted and shaken potentially making them valuable for biochemical sensors and catalytic nanoreactors.[40]

4. CONCLUSIONS

A simple technique to produce large-scale arrays of highly ordered ZnO nanorods was demonstrated. Three distinct ZnO crystal morphologies were prepared by use of different ZnO seed layers. For array formation, we used a simple variation on nanosphere lithography that patterns a thickness variation across a PMMA mask layer. Control of the etching time of the mask layer with an oxygen plasma enabled the tuning of the area of seed layer exposed. Subsequent hydrothermal growth produced high-quality ZnO crystals in uniform arrays. The high uniformity of the pattern was shown to induce the hydrophobic surface state without the need for chemical modification of the ZnO surface.

This combination of excellent individual crystal control and their arrangement into highly regular arrays suggests the possibility of using ZnO surfaces for micro-control of fluids. Some possibilities include: droplet control on the surface, biochemical sensors of small volumes, small-scale chemical reactors, and particle sorting at interfaces. Furthermore, this work encourages development in the integration of the excellent optical and electrical properties of high quality ZnO

nanorods into fluidic technologies to promote applications such as waterproof electronics and optofluidics.

AUTHOR INFORMATION

Corresponding Author

*E-mail: nichols@hanyang.ac.kr.

Notes

The authors declare no competing financial interest.

ACKNOWLEDGMENTS

This work was supported by a KIST research program (Gran 2E22121) and by the National Research Foundation of Korea (NRF) grant funded by the Korea government (MEST) (2011-0013704).

REFERENCES

(1) Hochbaum, A.I.; Yang, P. *Chem. Rev.* **2010**, *110*, 527−546.
(2) Wang, Z.L. *Mater. Sci. Eng., R* **2009**, *64*, 33−71.
(3) Yi, G.C.; Wang, C.; Park, W.I. *Semicond. Sci. Technol.* **2005**, *20*, s22−s34.
(4) Park, W.I.; Kim, D.H.; Jung, S.W.; Yi, G.C. *Appl. Phys. Lett.* **2002**, *80*, 4232−4234.
(5) Wang, X.; Summers, C.J.; Wang, Z.L. *Nano Lett.* **2004**, *4*, 423−426.
(6) Ravirajan, P.; Piero, A.M.; Nazeeruddin, M.K.; Graetzel, M.; Bradley, D.D.C.; Durrant, J.R.; Nelson, J. *J. Phys. Chem. B* **2006**, *110*, 7635−7639.
(7) Wang, X.; Song, J.L.; Wang, Z.L. *Science* **2007**, *316*, 102−105.
(8) Gonzalez-Valls, I.; Lira-Cantu, M. *Energy Environ. Sci.* **2009**, *2*, 19−34.
(9) Matsuu, M.; Shimada, S.; Masuya, K.; Hirano, S.; Kuwabara, M. *Adv. Mater.* **2006**, *18*, 1617−1621.
(10) Leem, J.W.; Song, Y.M.; Yu, J.S. *Nanotechnology* **2011**, *22*, 485304.
(11) Zhou, Q.; Zhao, J.; Xu, W.; Zhao, H.; Wu, Y.; Zheng, J. *J. Phys. Chem. C* **2008**, *112*, 2378−2381.
(12) Kwak, G.; Seol, M.; Tak, Y.; Yong, K. *J. Phys. Chem. C* **2009**, *113*, 12085−12089.
(13) Lee, S.; Kim, W.; Yong, K. *Adv. Mater.* **2011**, *23*, 4398−4402.
(14) Lee, W.W.; Yi, J.; Kim, S.B.; Kim, Y.H.; Park, H.G.; Park, W.I. *Cryst. Growth Des.* **2011**, *11*, 4927−4932.
(15) Banerjee, D.; Rybczynski, J.; Huang, J.Y.; Wang, D.Z.; Kempa, K.; Ren, Z.F. *Appl. Phys. A* **2005**, *80*, 749−752.
(16) Fan, H.J.; Fuhrmann, B.; Scholz, R.; Syrowatka, F.; Dadgar, A.; Krost, A.; Zacharias, M. *J. Crystal Growth* **2006**, *287*, 34−38.
(17) Liu, D.F.; Xiang, Y.J.; Liao, Q.; Zhang, J.P.; Wu, X.C.; Zhang, Z.X.; Liu, L.F.; Ma, W.J.; Shen, J.; Zhou, W.Y.; Xie, S.S. *Nanotechnology* **2007**, *18*, 405303.
(18) Zhang, X.; Liu, D.; Zhang, L.; Li, W.; Gao, M.; Ma, W.; Ren, Y.; Zeng, Q.; Niu, Z.; Zhou, W.; Xie, S. *J. Mater. Chem.* **2009**, *19*, 962−969.
(19) Li, C.; Hong, G.; Wang, P.; Yu, D.; Qi, L. *Chem. Mater.* **2009**, *21*, 891−897.
(20) Dong, J.J.; Zhang, X.W.; Yin, Z.G.; Zhang, S.G.; Wang, J.X.; Tan, H.R.; Gao, Y.; Si, F.T.; Gao, H.L. *ACS Appl. Mater. Interfaces* **2011**, *3*, 4388−4395.
(21) Lee, J.M.; Pyun, Y.B.; Yi, J.; Choung, J.W.; Park, W.I. *J. Phys. Chem. C* **2009**, *113*, 19134−19138.
(22) Alessandri, I.; Depero, L.E. *ACS Mater. Interface* **2011**, *2*, 594−602.
(23) Zhou, Q.; Zhao, J.; Xu, W.; Zhao, H.; Wu, Y.; Zheng, J. *J. Phys. Chem. C* **2008**, *112*, 2378−2381.
(24) Hale, M.S.; Mitchell, J.G. *Nano Lett.* **2001**, *1*, 617−620.
(25) Hale, M.S.; Mitchell, J.G. *Nano Lett.* **2002**, *2*, 657−660.
(26) Wood, T.J.; Hurst, G. A.; Schofield, W. C. E.; Thompson, R. L.; Oswald, G.; Evans, J. S. O.; Sharples, G. J.; Pearson, C.; Petty, M. C.; Badyal, J. P. S. *J. Mater. Chem.* **2012**, *22*, 3859−3867.
(27) Lee, W.W.; Kim, S.B.; Yi, J.; Nichols, W.T.; Park, W.I. *J. Phys. Chem C* **2012**, *116*, 456−460.
(28) Kwok, W.M.; Djurisic, A.B.; Leung, Y.H.; Li, D.; Tam, K.H.; Phillips, D.L.; Chan, W.K. *Appl. Phys. Lett.* **2006**, *89*, 183112.
(29) Myint, M.T.Z.; Kitsomboonloha, R.; Baruah, S.; Dutta, J. *J. Colloid Interface Sci.* **2011**, *354*, 810−815.
(30) Yoshimitsu, Z.; Nakajima, A.; Watanabe, T.; Hashimoto, K. *Langmuir* **2002**, *18*, 5818−5822.
(31) Quere, D. *Rep. Prog. Phys.* **2005**, *68*, 2495−2532.
(32) Barthlott, W.; Nienhius, C. *Planta* **1997**, *202*, 1−8.
(33) Wu, J.; Xia, J.; Lei, W.; Wang, B. *PLOS One* **2011**, *6*, e29047.
(34) Papadopoulou, E.L.; Barberoglou, M.; Zorba, V.; Manousaki, A.; Pagkozidis, A.; Stratakis, E.; Fotakis, C. *J. Phys. Chem. C* **2009**, *113*, 2891−2895.
(35) Wu, X.; Jiang, P.; Cai, W.; Bai, X.D.; Gao, P.; Xie, S.S. *Adv. Eng. Mater.* **2008**, *10*, 476−481.
(36) Wu, J.; Xia, J.; Lei, W.; Wang, B.P. *Mater. Lett.* **2011**, *65*, 477−479.
(37) Wang, D.; Liu, Y.; Liu, X.; Zhou, F.; Liu, W.; Xue, Q. *Chem. Commun.* **2009**, 7018−7020.
(38) Zhu, X.; Zhang, Z.; Men, X.; Yang, J.; Xu, X. *Appl. Surf. Sci.* **2010**, *256*, 7619−7622.
(39) Lai, Y.; Gao, X.; Zhuang, H.; Huang, J.; Lin, C.; Jiang, L. *Adv. Mater.* **2009**, *21*, 3799−3803.
(40) Jin, M.; Feng, X.; Feng, L.; Sun, T.; Zhai, J.; Li, T.; Jiang, L. *Adv. Mater.* **2005**, *17*, 1977−1981.